Published in final edited form as:
Langmuir. 2010 September 21; 26(18): 14747–14754. doi:10.1021/la1021438.

Structure and Order of Phosphonic Acid-Based Self-Assembled Monolayers on Si(100)

Manish Dubey[1,2], **Tobias Weidner**[1,3], **Lara J. Gamble**[1,3], and **David G. Castner**[1,2,3,*]

[1] National ESCA and Surface Analysis Center for Biomedical Problems, Box 351750, University of Washington, Seattle, WA 98195-1750 USA

[2] Department of Chemical Engineering, Box 351750, University of Washington, Seattle, WA 98195-1750 USA

[3] Department of Bioengineering, Box 351750, University of Washington, Seattle, WA 98195-1750 USA

Abstract

Organophosphonic acid self-assembled monolayers (SAMs) on oxide surfaces have recently seen increased use in electrical and biological sensor applications. The reliability and reproducibility of these sensors require good molecular organization in these SAMs. In this regard, packing, order and alignment in the SAMs is important, as it influences the electron transport measurements. In this study, we examine the order of hydroxyl- and methyl- terminated phosphonate films deposited onto silicon oxide surfaces by the tethering by aggregation and growth method using complementary, state-of-art surface characterization tools. Near edge x-ray absorption fine structure (NEXAFS) spectroscopy and *in situ* sum frequency generation (SFG) spectroscopy are used to study the order of the phosphonate SAMs in vacuum and under aqueous conditions, respectively. X-ray photoelectron spectroscopy and time of flight secondary ion mass spectrometry results show that these samples form chemically intact monolayer phosphonate films. NEXAFS and SFG spectroscopy showed that molecular order exists in the octadecylphosphonic acid and 11-hydroxyundecylphosphonic acid SAMs. The chain tilt angles in these SAMs were approximately 37° and 45°, respectively.

Keywords

Phosphonic acid; T-BAG method; NEXAFS; SFG; ToF-SIMS; XPS; surface analysis; order; SAM

Introduction

Self-assembled monolayers (SAMs) have been extensively studied and used in the last two decades due to their promise for controlling surface properties such as wettability, biocompatibility, corrosion resistance, as well as for their possible applications in electronic device fabrication and biosensors.[1, 2] Molecules capable of forming SAMs are composed of three basic units: 1) head groups which bind to the surface, 2) functional tail groups which are usually exposed at the SAM surfaces and can be used to tailor the chemical and physical properties of the surface, and 3) spacer chains which separate the head and tail groups and, in some cases, drive the self-assembly by lateral interactions between adjacent molecules.

*Corresponding Author: David G. Castner, castner@nb.engr.washington.edu.

A number of strategies for self-assembly have been developed in the past. The most common of these strategies involve thiols on noble metals (especially gold) and silanes on oxide surfaces. Thiol-based SAMs on gold are the most widely studied system due to the ease of sample preparation and uniformity of the films. They are extensively used as model systems in a wide range of studies.[3] Thiol-based SAMs function fine if the SAMs only needs to remain intact long enough to template a desired reaction (e.g., formation of an extracellular matrix overlayer in biological experiments). However, thiols tend to be oxidized or displaced from the surface with time, which makes thiol-based SAMs undesirable for applications that require long term stability.[4–6] Silanes on the other hand are more commonly used on oxide surfaces, where they can covalently bind to the surface by the transfer of a proton from the surface hydroxyl group to a silane leaving group, eliminating alcohol (in the case of ethoxysilanes) or HCl (in case of chlorosilanes). However, care must be taken to limit the film to a monolayer and avoid formation of 3-D silane networks.[7] In addition, some silane films have been shown to be hydrolytically unstable in aqueous base and unstable in biological media.[8] This can be a challenge for the applications that involve ambient conditions or biological environment.

Phosphonate head groups are a promising alternative for overcoming the limitations of thiol and silane systems since they are relatively robust and can be attached to a wide range of oxide surfaces. Phosphonic acid SAM formation has been reported on Al_2O_3,[9, 10] TiO_2,[11–13] ZrO_2,[14] planar mica[15] and SiO_2 [16–18] substrates, although proof of monolayer films was only provided in few cases.[16–18] Gawalt *et. al.*, discovered that adhesion and stability of phosphonic acid SAMs on TiO_2 is greatly enhanced by thermal annealing following the phosphonic acid film formation.[13, 19, 20] It was proposed that the phosphonic acid molecules in the unheated, as deposited film, are simply hydrogen-bonded to the substrate, and perhaps also to the neighboring molecules. The molecule-molecule interactions (van der Waals and H-bonding) are apparently stronger than substrate-molecule interactions in the deposited films. Heating the deposited film results in covalent attachment of the phosphonates to the substrate. The mechanism of growth of these films has been discussed in greater detail elsewhere.[20] Hanson *et al.*, built on this success and formulated a new technique to deposit the phosphonic acid films, referred to as the T-BAG (Tethering By Aggregation And Growth) method.[16] The phosphonate SAMs have been shown to have a better surface coverage and hydrolytic stability in alkaline conditions as compared to some types of silane films,[11, 21] as well as being stable under ambient conditions for a greater time period compared to thiols on gold,[22] likely owing to the P-O bond energy of ~80 kcal/mol compared to ~40 kcal/mol for the S-Au bond. These properties make phosphonate platforms very promising candidates for reallife applications that require long-term stability of the deposited monolayer. However, formation of the phosphate-based SAMs requires more extensive processing than formation of the thiol-based SAMs.

Phosphonic acid SAMs are increasingly used for building electronic thin-film devices due to their ability to form well defined and stable films on oxide surfaces.[23–27] Klauk *et al.* recently built ultralow-power organic circuits based on phosphonic acid SAMs and observed an order of magnitude decrease in the leakage current for phosphonic acid SAM devices compared to their silane counterpart.[23] Cattani-Scholz *et al.* have also shown excellent passivation properties of phosphonate SAM based devices.[27] They used the phosphonic acid monolayer for label free detection of DNA on silicon-on-insulator based flat surfaces as well as on nanowires. They discuss the uniformity of the phosphonate films for obtaining good passivation properties, which is very important for successful sensor development. A number of other groups are also utilizing the self-assembled phosphonic acid platform for various applications such as surface patterning,[28, 29] surface work function modification,[30, 31] small molecule detection,[32] corrosion inhibition,[33] biosensors,[34, 35] and electrical sensors.[23–27, 36] The importance of high film quality SAMs, i.e monolayers with a high packing

density, molecular alignment and binding uniformity, for use in molecular electronics is well established for thiol-based SAMs.[37–39] It has been shown in these studies that the packing and order greatly influences the electron transport measurements and the presence of molecular order is highly desirable for obtaining reproducible electronic properties.

Since the phosphonate SAMs are increasingly being used for applications in the field of electronic and bio-sensor development, it is important to study their order and uniformity. Although a number of characterization techniques, such as atomic force microscopy, quartz crystal microbalance, infrared, X-ray reflectivity, ellipsometry,[16–18, 27, 35, 40] have been used to understand the mechanism of phosphonate binding, the order, alignment, chemical integrity and uniformity of phosphonate-based films is yet to be investigated in detail. In this study, we probe the molecular order of methyl- and hydroxyl- terminated phosphonic acid SAMs on silicon. Near-edge X-ray absorption fine structure (NEXAFS) spectroscopy and sum-frequency generation (SFG) vibrational spectroscopy were used to investigate the conformation, alignment and ordering of the phosphonic acid films. The chemical composition and integrity of the films were examined using X-ray photoelectron spectroscopy (XPS) and time-of-flight secondary ion mass spectrometry (ToF-SIMS).

Experimental Section

SAM preparation

Phosphonate SAMs were formed using the T-BAG method. A detailed description of the deposition method has been presented elsewhere.[16] Briefly octadecylphosphonic acid (ODPA, $C_{18}H_{41}$-PO_3) or 11-hydroxyundecylphosphonic acid (PUL, $C_{11}H_{25}$-PO_4) (structures shown in Scheme 1) were self-assembled onto pre-cleaned (approximately 1×1 cm^2) silicon coupons by holding them vertically in a 25 μM solution of the acid in dry tetrahydrofuran (THF). The solvent was allowed to evaporate at room temperature and then coated coupons were heated in an oven at 140°C for 48 hours in air. The substrates are expected to still have phosphonic acid multilayers present on the surface after the heat treatment. Those multilayers were subsequently removed by cleaning the samples in THF. Three cycles of depositions with multiple rinsing and sonication in THF and methanol was used to produce a monolayer film. The films were stored in glass containers filled with nitrogen until they were characterized.

Octadeacanethiol (ODT, $C_{18}H_{37}$-SH) and mercaptoundecanol (MCU, $C_{11}OH_{23}$-SH) SAMs on gold were also prepared for comparison with their phosphonic acid counterparts. The thiol molecules where purchased from Asemblon (Redmond, USA). The gold substrates for the SAM fabrication were prepared by thermal evaporation of 200 nm gold (99.99% purity) onto polished single-crystal silicon (111) wafers (Silicon Sense) primed with a 5 nm titanium adhesion layer. The resulting films were polycrystalline with a grain size of 20–50 nm and expected to have predominantly a (111) orientation.[41] The films were formed by immersion of the freshly prepared gold substrates into 1 mM ethanol solutions of ODT or MCU at room temperature for 18 h. After immersion, the samples were carefully rinsed with copious amounts of ethanol, blown dry with nitrogen, and then kept in plastic or glass containers filled with nitrogen until they were characterized.

XPS analysis of the SAMs

XPS measurements were performed on a Kratos Axis Ultra DLD X-ray photoelectron spectrometer (Kratos Analytical, Manchester, UK) employing a hemispherical analyzer for spectroscopy and a spherical mirror analyzer for imaging. Spectra were acquired using a monochromatized Al-K_α X-ray source, a 90 degree photoelectron take-off angle from the surface, and the “hybrid” analysis mode. These experimental conditions result in a sampling depth of approximately 10 nm. A lowenergy electron flood gun was used to minimize

surface charging for silicon samples. XPS data were collected using an analysis area of 700 μm × 300 μm. For each sample, an initial compositional survey scan was acquired, followed by detailed elemental scans using a pass energy of 80 eV. High-resolution C 1s spectra were acquired using a pass energy of 20 eV and were charge-referenced to the C 1s hydrocarbon peak at 285.0 eV. Three spots on two replicates of each sample were analyzed. The intensities for each element were obtained by averaging the peak intensities determined from each spot. The average peak intensity was then divided by the appropriate relative sensitivity factor to correct for the orbital photoionization cross section and the instrument parameters. These normalized intensities for all the elements were then combined to obtain the compositional data. The reported compositions were not corrected for attenuation effects (e.g., attenuation of the S or P signals by the alkyl chains). Data analysis was performed with Vision Processing data reduction software (Kratos Analytical Ltd.) and CasaXPS (Casa Software Ltd.).

ToF-SIMS analysis of the SAMs

ToF-SIMS data for all the samples were acquired on an ION-TOF 5–100 instrument (ION-TOF GmbH, Münster, Germany) using a Bi_3^+ primary ion source. Positive and negative ion spectra were acquired from three spots on two replicates of each sample type with a pulsed 25 keV, 1.3 pA primary ion beam in the high current bunched mode (i.e., high mass resolution mode) from 100 μm × 100 μm areas on the sample surfaces. All data were collected using an ion dose below the static SIMS limit of 1×10^{12} ions/cm^2. The mass resolution ($m/\delta m$) of the negative secondary ion spectra was typically between 6000 and 7500 for the m/z = 25 peak. The $m/\delta m$ of the positive secondary ion spectra was typically between 7000 and 8500 for the m/z = 27 peak. Positive ion spectra were mass calibrated using the CH_3^+, $C_2H_3^+$, and $C_3H_5^+$ peaks. Negative ion mass spectra were mass calibrated using the CH^-, OH^- and C_2H^- peaks.

NEXAFS analysis of the SAMs

NEXAFS spectra were collected at the National Synchrotron Light Source (NSLS) U7A beamline at Brookhaven National Laboratory, using an elliptically polarized beam with ~85% *p*-polarization. This beam line uses a monochromator and 600 l/mm grating that provides a full-width at half-maximum (FWHM) resolution of ~0.15 eV at the carbon *K*-edge (285 eV). The monochromator energy scale was calibrated using the 285.35 eV C 1s $\rightarrow \pi^*$ transition on a graphite transmission grid placed in the path of the X-rays.[42] To eliminate the effect of incident beam intensity variation and monochromator absorption features, C *K*-edge spectra were normalized by the spectrum of a clean gold surface prepared by evaporation of gold in vacuo. Both the reference and signal were divided by the beam flux as a function of the photon energy prior to normalization.[43] Partial electron yield was monitored by a detector with the threshold voltage maintained at −150 V. Samples were mounted to allow rotation about the vertical axis to change the angle between the sample surface and the incident X-ray beam. The NEXAFS angle is defined as the angle between the incident X-ray beam and the sample surface.

SFG spectroscopy of modified silicon

The coherent, non-linear SFG spectra were obtained by overlapping visible and tunable IR laser pulses (25 ps) in time and space at incidence angles of 60° and 54°, respectively. The visible beam with a wavelength of 532 nm was delivered by an EKSPLA Nd:YAG laser operating at 50 Hz, which was also used to pump an EKSPLA optical parametric generation/amplification and difference frequency unit based on barium borate and $AgGaS_2$ crystals to generate tunable IR laser radiation from 1000 – 4000 cm^{-1}. The bandwidth was 1 cm^{-1} for the visible pump pulses and the IR laser. Both beams were only mildly focused and had a diameter of approximately 1 mm at the sample. The energy for each beam was 160 μJ per

pulse. The SFG signal generated at the sample was then analyzed by filters and a monochromator, detected with a gated photomultiplier tube and stored in a computer. The spectra were collected with 400 shots per data point in 2 cm^{-1} increments. A set of two replicates of each sample was analyzed. All spectra were recorded in *ppp* (sum, visible, and infrared) polarization combination along the [100] direction of the substrate. The SFG spectra were normalized by a reference SFG signal generated in a ZnS crystal. For the *in situ* study of the SAMs, the samples were soaked in deuterated water and then gently pressed against one side of an equilateral calcium fluoride prism and the surface of the sample was then probed going through the prism.

The intensity of the generated SF light I_{SF} is given by:

$$I_{SF} \propto |\chi^{(2)}_{eff}|^2 I_{IR} I_{vis} \tag{1}$$

here, I_{vis} and I_{IR} are the infrared and visible pump beam intensities, respectively, and $\chi^{(2)}_{eff}$ denotes the effective second-order nonlinear susceptibility of the interface which can be written as:[44]

$$I_{SFG} \propto |\chi^{(2)}|^2 = \left| \chi^{(2)}_{NR} + \sum_v \frac{A_v e^{i\varphi_v}}{\omega_{IR} - \omega_v + i\Gamma_v} \right|^2 \tag{2}$$

Here, $\chi^{(2)}_{NR}$ is the second order nonlinear susceptibility of the nonresonant background, $\boldsymbol{A}_v$ is the strength of the vth vibrational mode, φ_v denotes the phase of the respective mode and ω_{IR} refers to the frequency of the incident IR field. ω_v, $\boldsymbol{\Gamma}_v$ are the resonance position and width of the respective modes. Fitting eq 2 to the spectral data allows us to determine $\boldsymbol{A}_v$, ω_v and $\boldsymbol{\Gamma}_v$. In the fits, the Lorentzian line widths were set to 2 cm^{-1} and $\boldsymbol{\Gamma}_v$ was allowed to vary since the two contributions to the total line width could not be separated within the accuracy of the measurements.

Results and Discussion

X-ray Photoelectron Spectroscopy

The elemental composition of the SAMs was determined with XPS. The observed elemental composition of the SAMs can be compared to the stoichiometry of the phosphonic acid precursor molecules; which gives valuable information about the phosphonate attachment on the silicon oxide surface. Figure 1 shows the phosphorous region of the XP spectra before and after modifying the silicon surface with an ODPA monolayer. The peak near 191.0 eV (P 2s) observed after the film deposition shows that the phosphonic acid headgroups are present on the surface. A very similar spectrum was also obtained from the PUL modified surface. The broad peak at 184 eV is attributed to a bulk silicon plasmon peak. Plasmon loss features for silicon have been observed at binding energies 16.8 and 33.6 eV above the main peak.[45] Relative compositions, uncorrected for attenuation effects, of the ODPA and PUL modified silicon substrates along with ODT and MCU modified gold substrates are shown in Table 1. The C/P ratio for ODPA and PUL SAMs are approximately 21 and 15, respectively (Table 1), which is consistent with what other groups have observed on different substrates.[18, 46, 47] On the other hand, the C/S ratios for ODT and MCU SAMs are approximately 39 and 28, respectively (Table 1), suggesting that there is a greater attenuation of the sulfur signal compared to the phosphorous signal. Angle resolved XPS analysis has demonstrated

that the phosphorous is attached to the SiO_2 surface.[18] Thus the lower C/P ratios can be explained, at least in part, by a greater tilt angle (i.e., thinner organic overlayer) of the alkyl chains in the phosphonate SAMs compared to the thiol SAMs. The tilt angle of the phosphonate films is discussed in greater detail in the NEXAFS and SFG sections.

Differential charging analysis was utilized to confirm the presence of monolayers. Surface charging can result from the ejection of electrons during the XPS analysis. The further away from the silicon surface an atom is (e.g., carbon atoms in the multilayer region) the more difficult it will be to neutralize the residual positive charge on that atom. This results in a build-up of differential charging in the organic overlayer and a broadening of the XPS peaks from elements that are present in both the monolayer and multilayer regions.[17, 18] In this work, a C 1s spectrum is acquired before and after the multilayer cleaning procedure to confirm the presence of monolayer film. The broadening of the C 1s peak (shown in Figure 2 for ODPA) clearly evident in the multilayer sample corresponds to adsorbed multilayers on the surface. A single, narrow C 1s peak (FWHM = 1.2 eV) was observed after ultrasonic cleaning of the samples in the organic solvents, consistent with removal of the adsorbed multilayers, and confirming the presence of a monolayer.

Time of Flight Secondary Ion Mass Spectrometry

ToF-SIMS was conducted on the freshly cleaned silicon samples along with phosphonic acid modified substrates. The main positive fragments from the reference spectra (obtained from freshly cleaned silicon) consisted of silicon (e.g., Si^+) and silicon oxides (e.g., $SiOH^+$, Si_2O^+) along with small amount of hydrocarbon contamination (e.g., $C_nH_{2n+1}{}^+$ and $C_nH_{2n-1}{}^+$). The negative spectrum of the reference sample mainly consisted of O^- and OH^- peaks along with some hydrocarbon contamination and substrate peaks (CH^-, C_2H^-, SiO^-, $SiO_2{}^-$ etc.). The silicon samples modified with ODPA clearly showed the presence of bound phosphonates in the positive spectrum (e.g., $SiPO_2{}^+$). In addition the peak at 335.27 ($C_{18}H_{40}PO_3{}^+$) represents a molecular ion ($M+H^+$) and another peak at 361.23 ($SiC_{18}H_{38}PO_3{}^+$) indicates the formation of bound phosphonate monolayers on the surface. The negative spectrum also shows a molecular ion ($M-H^-$) at 333.26 ($C_{18}H_{38}PO_3{}^-$) and a peak at 377.23 ($SiC_{18}H_{38}PO_4{}^-$) that indicates the formation of bound phosphonate monolayers on the surface (Figure 3). Similarly for the hydroxyl terminated phosphonic acid monolayers, the molecular mass peak was observed in the negative spectrum at 251.14 ($C_{11}H_{24}O_4P^-$). Additional peaks in the negative spectra of both the samples at 106.93 ($SiPO_3{}^-$), 134.96 ($SiPO_3C_2H_4{}^-$) and 162.99 ($SiPO_3C_4H_8{}^-$) indicate that the phosphate films are bound on the surface (Figure 4). Table 2 shows all the characteristic positive and negative fragments observed from SAMs of ODPA and PUL. Similar fragments have been observed from a phosphonic acid modified titanium oxide surface[35] and have been shown to be indicative of monolayer formation in several other studies.[48, 49]

NEXAFS Spectroscopy

Valuable information about the chemical bonding and the alignment of the SAMs is provided by NEXAFS spectroscopy. This technique gives insight into the electronic structure of the films by sampling unoccupied molecular orbitals.[43] It can provide molecular orientation from the x-ray linear dichroism by measuring the change in absorption resonance intensities as a function of the orientation of the x-ray electric field vector with respect to the sample surface.

C *K*-edge spectra of PUL, ODPA and a reference ODT SAM (known to yield well aligned films on gold surfaces) acquired at X-ray incidence angles of 70°, 55° and 20° are presented in Figure 5 along with the difference between 70° and 20° spectra. All spectra contain resonance peaks superimposed onto an adsorption edge related to excitation of C 1s electron

into continuum states. Both the ODPA and PUL spectra exhibit a sharp resonance at ~287.6 eV (R*/C-H σ*) and two broader resonances at ~293.3 eV (C-C σ*) and 301.3 eV (C-C′ σ*) expected from hydrocarbon chains.[43, 50–52] A very weak peak at ~285.2 eV is also observed. This peak is tentatively assigned to an excitation into alkane-substrate orbitals,[53, 54] or a minor normalization issue caused by carbon contamination on the beamline optics. Since radiation damage from the x-rays can also cause peaks to appear in this spectral range, a careful beam damage study was performed to rule out this possibility. The 280 to 290 eV energy range was repeatedly scanned and the partial electron yield at 285.2 eV was monitored over time to rule out damage related changes. No changes in the spectra were observed within 15 minutes, which is longer than the exposure time needed to acquire a full C *K*-edge spectrum from these samples. Thus, all resonances expected for intact ODPA and PUL monolayers were present in the spectra and no contamination related features, e.g. C=O species which are often seen in loosely packed films, were observed.

The shape of the 70° − 20° difference spectra for the ODPA and the PUL films is similar to the observed dichroism for the ODT SAM. Both show positive and negative peaks for the R* and σ* resonances, respectively. The molecular orbitals related to the R* transition are oriented perpendicular to the alkyl chains while those related to transitions into the C-C and C-C′ σ* orbitals are oriented parallel to the chain. Consequently, from the sign of the difference spectra, the molecular orientation of both the PUL and the ODPA SAM is determined to be mostly upright.[43] However, the intensity of the difference peaks is significantly weaker for the two phosphonic acid-based SAMs when compared to the ODT SAM. The difference in intensities in the SAMs can be quantified by using the variation of the R*/C-H σ* resonance intensities with the X-ray incidence angle α. We here define the dichroic ratio R_I as:

$$R_I = \frac{I_{70^\circ} - I_{0^\circ}}{I_{70^\circ} + I_{0^\circ}} \tag{3}$$

where I_{70° is the intensity at α=70° and I_{0° is the intensity at α=0°, extrapolated from a plot of the R*/C-H σ* resonance intensities against $\sin^2(\alpha)$.[55] The obtained R_I for ODPA and PUL are summarized in Figure 6, along with those for their thiol-based counterparts (ODT and MCU on gold) as references. A larger positive R_I value corresponds to a more upright orientation of the alkane chains and a negative value indicates a strongly tilted or disordered conformation. For disordered, amorphous films R_I will be 0. The value of 0.58 observed here for the ODT reference shows the films is densely packed and crystalline. The MCU reference shows a somewhat lower R_I value (0.35), which has been observed before[56] and can be explained by the shorter alkane chain compared to ODT and, thus, lower film crystallinity.[57] The ODPA film exhibits a R_I value of 0.32, which is significantly lower than its counterpart ODT. The R_I value observed for PUL is even lower (0.11). The lower R_I values for the phosphonic acid-based films compared to the thiol systems can be due to either a more tilted conformation or a higher degree of disorder. The similar chain length R_I dependence for the thiol systems (R_I(ODT)− R_I(MCU)=0.23) and the phosphonic acid systems (R_I(ODPA) − R_I(PUL)=0.20) indicates that the lower R_I values come from a generally higher tilt angle for the phosphonic acid-based films which can be explained by a different head group – substrate bond angle (i.e., phosphonate-oxide vs. thiol-gold) and surface potential corrugation.[58–62] This view is also supported by the SFG analysis discussed below.

A qualitative evaluation of the angular dependence of the R*-resonances within the standard theoretical framework[43] yields a hydrocarbon chain tilt angle of 37° and 47° for ODPA and PUL, respectively. As expected, the tilt angle value for ODPA is significantly higher than

for its counterpart alkanethiol SAM on gold (28° for the present data set). A tilt angle of 40° for ODPA films deposited onto a silicon oxide surface has been estimated by AFM and X-ray reflectivity studies.[16] For the PUL film, ellipsometry has been used by others to estimate a tilt angle of approximately 52°.[27] As discussed, the calculated angle for PUL may be affected by a lower degree of ordering in that film. However, the tilt angle is still smaller than the 55° NEXAFS angle characteristic of completely disordered layers.[43] The observed tilt angles suggest a thickness of 1.8 and 1.2 nm for ODPA and PUL respectively (estimated molecule length; ODPA ~2.4 nm, PUL ~1.7 nm).

SFG Spectroscopy

Since a broad variety of possible applications for phosphonic acid-based SAMs involves their exposure to ambient or biologically relevant conditions, a complementary *in situ* analysis of the film structure was performed in deuterated water using SFG spectroscopy. Spectra of PUL and ODPA SAMs in deuterated water along with the corresponding fits of the SFG equation are shown in Figure 7. The ODPA spectrum exhibits the expected three peaks from the terminal methyl's at 2965 cm^{-1} (r^-), 2940 cm^{-1} (r^-_{FR}), and 2880 cm^{-1} (r^+) which are commonly related to a well ordered and densely packed SAM, supporting our view that the high tilt angles for phosphonic acid-based SAMs compared to thiol on gold are not explained by a more amorphous film structure.[63] A spectrum of ODT on gold is also shown in Figure 7 to compare the quality of the phosphonate films to their thiol counterparts.

The CH_2 related stretching resonances visible near 2860 (d^+) and near 2916 cm^{-1} (d^-) indicate a noticeable amount of trans-gauche defects in the phosphonate SAM backbone.[63, 64] These defects are not visible in the reference ODT SAM spectrum and are possibly introduced into the phosphonate SAMs by the vigorous sonication of the samples in organic solvents for the removal of multilayers from the surface. This indicates that the phosphonate SAMs are not as well packed as the thiol-based film. Note that the shape of the methyl related peaks differs significantly from the methylene resonances because of the different phase (i.e., interference pattern) of the former signal with respect to the nonresonant background of the Si(100) substrate. The resonance positions discussed here are obtained from fits of the SFG equation.

The PUL SFG spectrum shows three strong vibrational modes: The resonance near 2860 cm^{-1} that has been assigned to the d^+ CH stretch mode and two features at around 2885 cm^{-1} and 2941 cm^{-1} which can be assigned to symmetric and asymmetric stretches of the methylene unit adjacent to the terminal hydroxyl group respectively. We note that the methylene next to the phosphonic acid linker is located next to a phosphorous atom, and thus could also be the source of the blue-shifted signal. However, since these resonances are not observed in ODPA, which has the same linker but lacks a terminal OH group, the latter possibility is less likely here. A blue-shift of vibrational modes due to interaction with OH groups is well established in the SFG and IR literature. [65–67] The SFG signals of neighboring methylene units in the central portion of the chain cancel out because of the symmetric environment of the molecular units. The shifted modes of the methylene unit next to the OH groups do not cancel out since it is not in a symmetric environment. The presence of these modes in the SFG spectrum indicates significant order is present at the surface of the PUL SAM.[63, 68]

The tilt angles for the films were calculated from the symmetric and asymmetric C-H_3 modes for ODPA and the CH_2 stretches related to the methylene unit neighboring the terminal hydroxyl group for PUL using published procedures[69] and the theoretical framework described in refs [70] and [71]. The obtained chain tilt angles from the surface

normal were 38° and 43° for the ODPA and PUL SAMs, respectively. Both agree closely with the NEXAFS results.

Figure 8 displays *in situ* SFG spectra of ODPA and PUL taken in the fingerprint region between 1600 cm^{-1} and 1000 cm^{-1}. Both spectra are dominated by a strong resonance near 1400 cm^{-1} most likely related to a deformation vibration (CH_2-def) of the methylene adjacent to the phosphorous atom of the head group. The feature is pronounced in both spectra and is probably an indicator of a well-ordered layer of phosphonic acid headgroups in both SAMs. In the spectrum of ODPA, the CH_2-def resonance is accompanied by weak but discernible features near 1196 cm^{-1} and 1474 cm^{-1}. The former mode is likely related to the PO_3^{2-} group, while the latter resonance can be assigned either to deformation vibrations of CH_2 and CH_3, or alternatively to P=O stretching vibrations.[72] Conversely, both peaks are absent in the PUL spectra, indicating a mostly disordered headgroup layer for this SAM. This lower degree of molecular alignment in the PUL SAM compared to ODPA is consistent with the CH SFG data and the NEXAFS analysis.

Conclusions

Phosphonic acid-based SAMs are becoming widely used in the modification of oxide surfaces for electrical sensor applications. We have studied the order of alkylphosphonic acid SAMs on silicon oxide surfaces fabricated by the T-BAG method. We have also presented thiol counterparts of these SAMs on gold for a head-to-head comparison of their molecular order and uniformity. NEXAFS spectroscopy was used to study the order of methyl- and hydroxyl- terminated phosphonate SAMs in vacuum. SFG spectroscopy provided complementary order analysis under aqueous conditions. XPS and ToF-SIMS analysis of these samples confirm the presence of chemically intact phosphonate monolayers. NEXAFS spectroscopy indicate molecular order in the ODPA and PUL films with tilt angles of 37° and 47°, respectively. The order in these films is very comparable to the reference ODT and MCU films deposited onto gold. SFG studies in deuterated water showed similar tilt angles (38° and 43°, respectively). The ODPA SFG spectra exhibited peaks from the terminal methyl units, which is consistent with ordered films. However, a noticeable degree of trans-gauche defects was also evident, possibly due to the extensive sonication of the samples in organic solvents for the removal of multilayer films. PUL films also showed a considerable degree of alignment as indicated by resonances of the methylene unit next to the terminal hydroxyl group. The presence of a peak at 1400 cm^{-1} in both the films indicates an array of very well-ordered phosphonate groups. These studies show that well ordered SAMs with methyl or hydroxyl termination can be prepared on oxide surfaces using phosphonate headgroups.

Acknowledgments

The authors thank Prof. Jeffrey Schwartz from Princeton University for providing the PUL molecules. XPS analysis of the reference ODT and MCU SAMs by Joe Baio and Nicolas Vandencasteele (University of Washington) is gratefully acknowledged. This research was supported by the National ESCA and Surface Analysis Center for Biomedical Problems (NIH grant EB-002027). TW thanks the Deutsche Forschungsgemeinschaft for a research fellowship. We thank Daniel Fischer (NIST) and Cherno Jaye (Hunter College) for providing us with the experimental equipment for NEXAFS spectroscopy and their technical assistance at the synchrotron. NEXAFS studies were performed at the NSLS, Brookhaven National Laboratory, which is supported by the U.S. Department of Energy, Division of Materials Science and Division of Chemical Sciences.

References

1. Chapman RG, Ostuni E, Yan L, Whitesides GM. Preparation of mixed self-assembled monolayers (SAMs) that resist adsorption of proteins using the reaction of amines with a SAM that presents interchain carboxylic anhydride groups. Langmuir. 2000; 16 (17):6927–6936.

2. Mrksich M. A surface chemistry approach to studying cell adhesion. Chem Soc Rev. 2000; 29 (4): 267–273.
3. Chechik, V.; Striling, CJM. Gold-thiol self-assembled monolayers. In: Patai, S.; Rappoport, Z., editors. The chemistry of Organic Derivatives of Gold and Silver. Wiley Interscience; 1999.
4. Flynn NT, Tran TNT, Cima MJ, Langer R. Long-term stability of self-assembled monolayers in biological media. Langmuir. 2003; 19 (26):10909–10915.
5. Sung IH, Kim DE. Surface damage characteristics of self-assembled monolayers of alkanethiols on metal surfaces. Tribology Letters. 2004; 17 (4):835–844.
6. Willey TM, Vance AL, van Buuren T, Bostedt C, Terminello LJ, Fadley CS. Rapid degradation of alkanethiol-based self-assembled monolayers on gold in ambient laboratory conditions. Surf Sci. 2005; 576 (1–3):188–196.
7. Mutin PH, Guerrero G, Vioux A. Hybrid materials from organophosphorus coupling molecules. J Mater Chem. 2005; 15 (35–36):3761–3768.
8. Xiao SJ, Textor M, Spencer ND, Sigrist H. Covalent attachment of cell-adhesive, (Arg-Gly-Asp)-containing peptides to titanium surfaces. Langmuir. 1998; 14 (19):5507–5516.
9. Lewington TA, Alexander MR, Thompson GE, McAlpine E. Bodycote Prize Paper Characterisation of alkyl phosphonic acid monolayers self assembled on hydrated surface of aluminium. Surf Eng. 2002; 18 (3):228–232.
10. Hauffman T, Blajiev O, Snauwaert J, van Haesendonck C, Hubin A, Terryn H. Study of the Self-Assembling of n-Octylphosphonic Acid Layers on Aluminum Oxide. Langmuir. 2008; 24 (23): 13450–13456. [PubMed: 18973311]
11. Silverman BM, Wieghaus KA, Schwartz J. Comparative properties of siloxane vs phosphonate monolayers on a key titanium alloy. Langmuir. 2005; 21 (1):225–228. [PubMed: 15620307]
12. Zorn G, Gotman I, Gutmanas EY, Adadi R, Salitra G, Sukenik CN. Surface modification of Ti45Nb alloy with an alkylphosphonic acid self-assembled monolayer. Chem Mater. 2005; 17 (16):4218–4226.
13. Gawalt ES, Lu G, Bernasek SL, Schwartz J. Enhanced bonding of alkanephosphonic acids to oxidized titanium using surface-bound alkoxyzirconium complex interfaces. Langmuir. 1999; 15 (26):8929–8933.
14. Gao W, Reven L. Solid-State Nmr-Studies of Self-Assembled Monolayers. Langmuir. 1995; 11 (6):1860–1863.
15. Woodward JT, Ulman A, Schwartz DK. Self-assembled monolayer growth of octadecylphosphonic acid on mica. Langmuir. 1996; 12 (15):3626–3629.
16. Hanson EL, Schwartz J, Nickel B, Koch N, Danisman MF. Bonding self-assembled, compact organophosphonate monolayers to the native oxide surface of silicon. J Am Chem Soc. 2003; 125 (51):16074–16080. [PubMed: 14677999]
17. Dubey M, Gouzman I, Bernasek SL, Schwartz J. Characterization of self-assembled organic films using differential charging in X-ray photoelectron spectroscopy. Langmuir. 2006; 22 (10):4649–4653. [PubMed: 16649777]
18. Gouzman I, Dubey M, Carolus MD, Schwartz J, Bernasek SL. Monolayer vs. multilayer self-assembled alkylphosphonate films: X-ray photoelectron spectroscopy studies. Surface Science. 2006; 600 (4):773–781.
19. Gawalt ES, Avaltroni MJ, Koch N, Schwartz J. Self-assembly and bonding of alkanephosphonic acids on the native oxide surface of titanium. Langmuir. 2001; 17 (19):5736–5738.
20. Gawalt ES, Brault-Rios K, Dixon MS, Tang DC, Schwartz J. Enhanced bonding of organometallics to titanium via a titanium(III) phosphate interface. Langmuir. 2001; 17 (21):6743–6745.
21. Marcinko S, Fadeev AY. Hydrolytic stability of organic monolayers supported on TiO2 and ZrO2. Langmuir. 2004; 20 (6):2270–2273. [PubMed: 15835682]
22. Mani G, Johnson DM, Marton D, Dougherty VL, Feldman MD, Patel D, Ayon AA, Agrawal CM. Stability of self-assembled monolayers on titanium and gold. Langmuir. 2008; 24 (13):6774–6784. [PubMed: 18512878]
23. Klauk H, Zschieschang U, Pflaum J, Halik M. Ultralow-power organic complementary circuits. Nature. 2007; 445 (7129):745–748. [PubMed: 17301788]

24. McDermott JE, McDowell M, Hill IG, Hwang J, Kahn A, Bernasek SL, Schwartz J. Organophosphonate self-assembled monolayers for gate dielectric surface modification of pentacene-based organic thin-film transistors: A comparative study. J Phys Chem A. 2007; 111 (49):12333–12338. [PubMed: 17997528]
25. McDowell M, Hill IG, McDermott JE, Bernasek SL, Schwartz J. Improved organic thin-film transistor performance using novel self-assembled monolayers. Appl Phys Lett. 2006; 88(7)
26. Hanson EL, Guo J, Koch N, Schwartz J, Bernasek SL. Advanced surface modification of indium tin oxide for improved charge injection in organic devices. J Am Chem Soc. 2005; 127 (28): 10058–10062. [PubMed: 16011369]
27. Cattani-Scholz A, Pedone D, Dubey M, Neppl S, Nickel B, Feulner P, Schwartz J, Abstreiter G, Tornow M. Organophosphonate-based PNA-functionalization of silicon nanowires for label-free DNA detection. ACS Nano. 2008; 2 (8):1653–1660. [PubMed: 19206369]
28+. Bardecker JA, Afzali A, Tulevski GS, Graham T, Hannon JB, Jen AKY. Directed assembly of single-walled carbon nanotubes via drop-casting onto a UV-patterned photosensitive monolayer. J Am Chem Soc. 2008; 130(23):7226. [PubMed: 18481849]
29. Hannon JB, Afzali A, Klinke C, Avouris P. Selective placement of carbon nanotubes on metal-oxide surfaces. Langmuir. 2005; 21 (19):8569–8571. [PubMed: 16142926]
30. Koh SE, McDonald KD, Holt DH, Dulcey CS, Chaney JA, Pehrsson PE. Phenylphosphonic acid functionalization of indium tin oxide: Surface chemistry and work functions. Langmuir. 2006; 22 (14):6249–6255. [PubMed: 16800683]
31. Guo J, Koch N, Schwartz J, Bernasek SL. Direct measurement of surface complex loading and surface dipole and their effect on simple device behavior. J Phys Chem B. 2005; 109 (9):3966–3970. [PubMed: 16851451]
32+. Dubey M, Bernasek SL, Schwartz J. Highly sensitive nitric oxide detection using X-ray photoelectron spectroscopy. J Am Chem Soc. 2007; 129(22):6980. [PubMed: 17497778]
33. Quinones R, Gawalt ES. Polystyrene formation on monolayer-modified nitinol effectively controls corrosion. Langmuir. 2008; 24 (19):10858–10864. [PubMed: 18763818]
34. Luo W, Westcott NP, Pulsipher A, Yousaf MN. Renewable and Optically Transparent Electroactive Indium Tin Oxide Surfaces for Chemoselective Ligand Immobilization and Biospecific Cell Adhesion. Langmuir. 2008; 24 (22):13096–13101. [PubMed: 18928305]
35. Adden N, Gamble LJ, Castner DG, Hoffmann A, Gross G, Menzel H. Phosphonic acid monolayers for binding of bioactive molecules to titanium surfaces. Langmuir. 2006; 22 (19):8197–8204. [PubMed: 16952262]
36. Zschieschang U, Halik M, Klauk H. Microcontact-printed self-assembled monolayers as ultrathin gate dielectrics in organic thin-film transistors and complementary circuits. Langmuir. 2008; 24 (5):1665–1669. [PubMed: 18198917]
37. Dhirani AA, Zehner RW, Hsung RP, Guyot-Sionnest P, Sita LR. Self-assembly of conjugated molecular rods: A high-resolution STM study. J Am Chem Soc. 1996; 118 (13):3319–3320.
38. Noh J, Park H, Jeong Y, Kwon S. Structure and electrochemical behavior of aromatic thiol self-assembled monolayers on Au(111). Bull Korean Chem Soc. 2006; 27 (3):403–406.
39. Dholakia GR, Fan W, Meyyappan M. Effect of monolayer order and dynamics on the electronic transport of molecular wires. Applied Physics a-Materials Science & Processing. 2005; 80 (6): 1215–1223.
40. Raman A, Dubey M, Gouzman I, Gawalt ES. Formation of self-assembled monolayers of alkylphosphonic acid on the native oxide surface of SS316L. Langmuir. 2006; 22 (15):6469–6472. [PubMed: 16830984]
41. Heister K, Zharnikov M, Grunze M, Johansson LSO. Adsorption of Alkanethiols and Biphenylthiols on Au and Ag Substrates: A High-Resolution X-ray Photoelectron Spectroscopy Study. J Phys Chem B. 2001; 105 (19):4058–4061.
42. Batson PE. Carbon 1s near-edge-absorption fine structure in graphite. Phys Rev B. 1993; 48 (4): 2608.
43. Stöhr, J. NEXAFS Spectroscopy. Vol. 25. Springer-Verlag; Berlin: 1992.
44. Bain CD, Davies PB, Ong TH, Ward RN, Brown MA. Quantitative-Analysis of Monolayer Composition by sum-frequency vibrational spectroscopy. Langmuir. 1991; 7 (8):1563–1566.

45. Abbate M, Alonso EV. Plasmon Production in the X-Ray Photoelectron-Spectra of Ar and K Implanted in Al and Si. Journal of Physics-Condensed Matter. 1989; 1 (10):1929–1932.
46. Hoque E, DeRose JA, Hoffmann P, Mathieu HJ, Bhushan B, Cichomski M. Phosphonate self-assembled monolayers on aluminum surfaces. J Chem Phys. 2006; 124(17)
47. Spori DM, Venkataraman NV, Tosatti SGP, Durmaz F, Spencer ND, Zurcher S. Influence of alkyl chain length on phosphate self-assembled monolayers. Langmuir. 2007; 23 (15):8053–8060. [PubMed: 17569549]
48. Lu G, Bernasek SL, Schwartz J. Oxidation of a polycrystalline titanium surface by oxygen and water. Surf Sci. 2000; 458 (1–3):80–90.
49. Tosatti S, Michel R, Textor M, Spencer ND. Self-assembled monolayers of dodecyl and hydroxy-dodecyl phosphates on both smooth and rough titanium and titanium oxide surfaces. Langmuir. 2002; 18 (9):3537–3548.
50. Outka DA, Stöhr J, Rabe JP, Swalen JD. The orientation of Langmuir-Blodgett monolayers using NEXAFS. J Chem Phys. 1988; 88 (6):4076.
51. Weiss K, Bagus PS, Wöll C. Rydberg transitions in X-ray absorption spectroscopy of alkanes: The importance of matrix effects. J Chem Phys. 1999; 111 (15):6834–6845.
52. Väterlein P, Fink R. Analysis of the x-ray absorption spectra of linear saturated hydrocarbons using the Xa scattered-wave method. J Chem Phys. 1998; 108 (8):3313.
53. Cabarcos OM, Shaporenko A, Weidner T, Uppili S, Dake LS, Zharnikov M, Allara DL. Physical and Electronic Structure Effects of Embedded Dipoles in Self-Assembled Monolayers: Characterization of Mid-Chain Ester Functionalized Alkanethiols on Au{111}. J Phys Chem C. 2008; 112 (29):10842–10854.
54. Witte G, Weiss K, Jakob P, Braun J, Kostov KL, Wöll C. Damping of Molecular Motion on a Solid Substrate: Evidence for Electron-Hole Pair Creation. Phys Rev Lett. 1998; 80 (1):121.
55. Sambasivan S, Hsieh S, Fischer DA, Hsu SM. J Vac Sci Technol, A. 2006; 24:1484.
56. DelRio FW, Steffens KL, Jaye C, Fischer DA, Cook RF. Elastic, Adhesive, and Charge Transport Properties of a Metal-Molecule-Metal Junction: The Role of Molecular Orientation, Order, and Coverage. Langmuir. 2010; 26 (3):1688–1699. [PubMed: 19839640]
57. Strong LW, Gerge M. Structures of self-assembled monolayer films of organosulfur compounds adsorbed on gold single crystals: electron diffraction studies. Langmuir. 1988; 4:546–558.
58. Laibinis PE, Whitesides GM, Allara DL, Tao YT, Parikh AN, Nuzzo RG. Comparison of the structures and wetting properties of self-assembled monolayers of n-alkanethiols on the coinage metal surfaces, copper, silver, and gold. J Am Chem Soc. 1991; 113 (19):7152–7167.
59. Weidner T, Shaporenko A, Ballav N, Ulman A, Zharnikov M. Modification of Alkaneselenolate Monolayers by Low-Energy Electrons. Journal of Physical Chemistry C. 2008; 112 (4):1191–1198.
60. Shaporenko ABM, Terfort A, Johansson LSO, Grunze M, Zharnikov M. Odd-Even Effects in Photoemission from Terphenyl-Substituted Alkanethiolate Self-Assembled Monolayers. Langmuir. 2005; 21 (10):4370–4375. [PubMed: 16032849]
61. Shaporenko AMJ, Weidner T, Terfort A, Zharnikov M. Balance of Structure-Building Forces in Selenium-Based Self-Assembled Monolayers. J Am Chem Soc. 2007
62. Rong HTFS, Yang Y-J, Zharnikov M, Buck M, Wuhn M, Wöll C, Helmchen G. On the Importance of the Headgroup Substrate Bond in Thiol Monolayers: A Study of Biphenyl-Based Thiols on Gold and Silver. Langmuir. 2001; 17 (5):1582–1593.
63. Himmelhaus M, Eisert F, Buck M, Grunze M. Self-Assembly of *n*-Alkanethiol Monolayers. A Study by IR-Visible Sum Frequency Spectroscopy (SFG). J Phys Chem B. 2000; 104:576–584.
64. Palyvoda O, Bordenyuk AN, Yatawara AK, McCullen E, Chen CC, Benderskii AV, Auner GW. Molecular organization in SAMs used for neuronal cell growth. Langmuir. 2008; 24 (8):4097–4106. [PubMed: 18338909]
65. Sartenaer, Y.; Tourillon, G.; Dreesen, L.; Lis, D.; Mani, AA.; Thiry, PA.; Peremans, A. Sum-frequency generation spectroscopy of DNA monolayers. Biosensors and Bioelectronics; Selected Papers from the Ninth World Congress On Biosensors; Toronto, Canada. 10 – 12 May 2006; 2007. p. 2179-2183.Alice X J Tang

66. Lin-Vien, DC.; Norman, B.; Fately William, G.; Grasselli Jeanette, G. The Handbook of Infrared and Raman Characteristic Frequencies of Organic Molecules. Academic Press; San Diego, CA: 1991.

67. Asanuma H, Noguchi H, Uosaki K, Yu HZ. Structure and reactivity of alkoxycarbonyl (ester)-terminated monolayers on silicon: Sum frequency generation spectroscopy. J Phys Chem B. 2006; 110 (10):4892–4899. [PubMed: 16526728]

68. Lambert AG, Davies PB, Neivandt DJ. Implementing the Theory of Sum Frequency Generation Vibrational Spectroscopy: A Tutorial Review. Appl Spectrosc Rev. 2005; 40:103–145.

69. Nishi N, Hobara D, Yamamoto M, Kakiuchi T. Chain-length-dependent change in the structure of self-assembled monolayers of n-alkanethiols on Au(111) probed by broad-bandwidth sum frequency generation spectroscopy. J Chem Phys. 2003; 118 (4):1904–1911.

70. Zhuang X, Miranda PB, Kim D, Shen YR. Mapping molecular orientation and conformation at interfaces by surface nonlinear optics. Phys Rev B. 1999; 59 (19):12632–12640.

71. Bain CD. Sum-Frequency Vibrational Spectroscopy of the Solid/Liquid Interface. J Chem Soc Faraday Trans. 1995; 91 (9):1281–1296.

72. Bellamy, LD. The infra-red spectra of complex molecules. 3. Lowe & Brydone; Thetford, Norfolk: 1975.

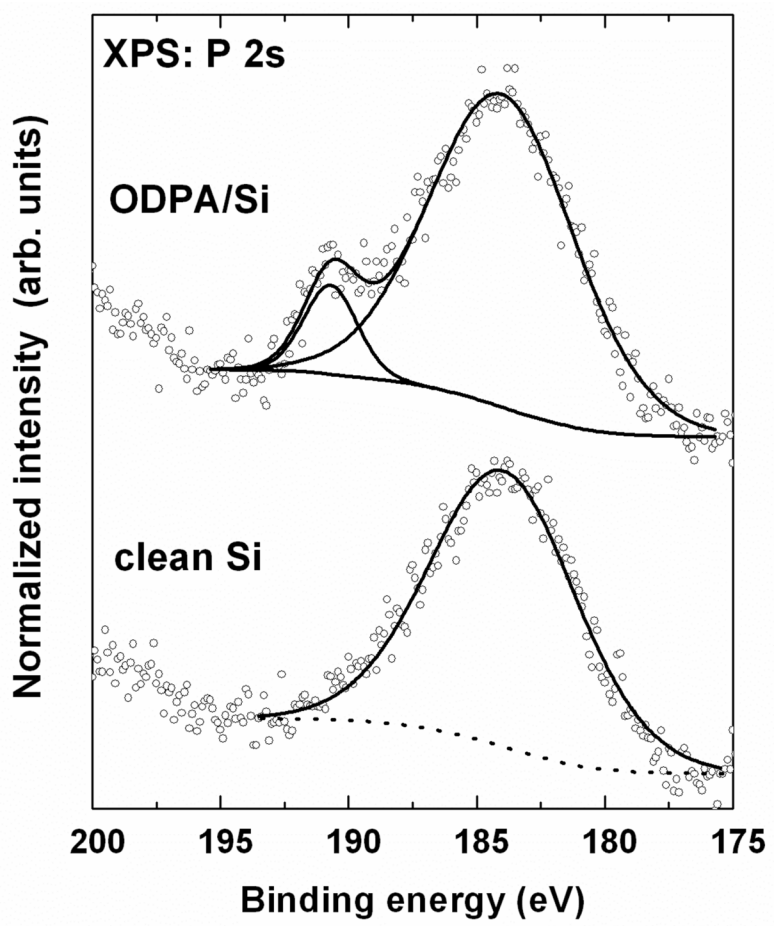

Figure 1.
XPS P 2s spectra of clean (bottom) and ODPA modified (top) silicon substrates. The peak at 191.0 eV is characteristic of phosphonate species in the film. The broad peak near 184 eV is a silicon bulk plasmon loss feature.

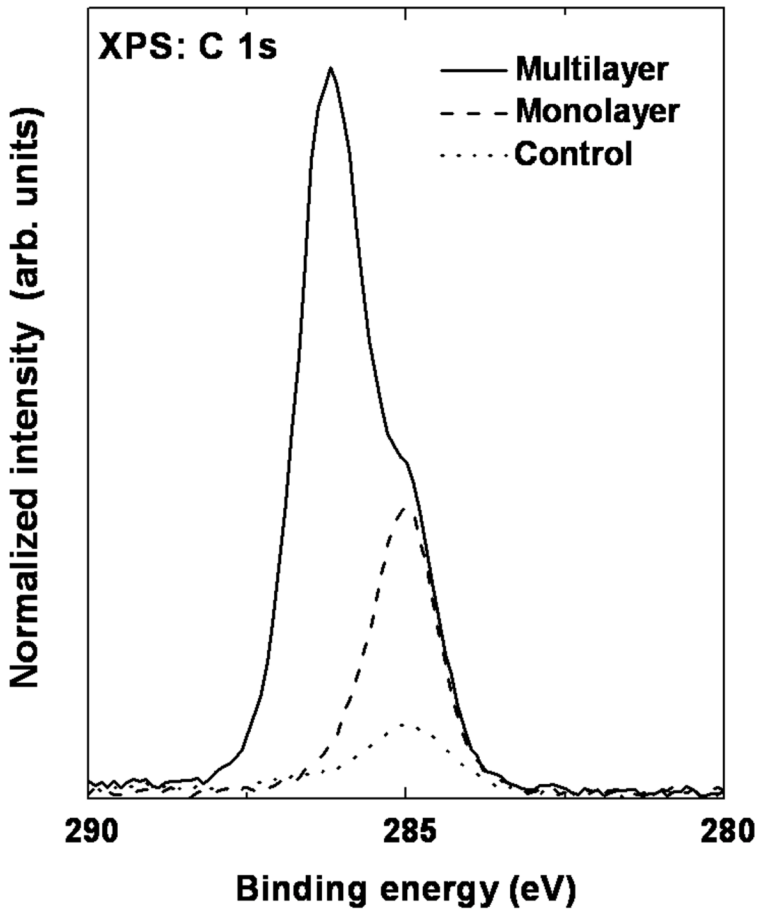

Figure 2.
C 1s XPS region of mono and multi-layer films of ODPA on silicon along with a spectrum of clean silicon. The broadening of the C 1s peak is a result of the presence of organic multilayers causing differential charging within the overlayer.

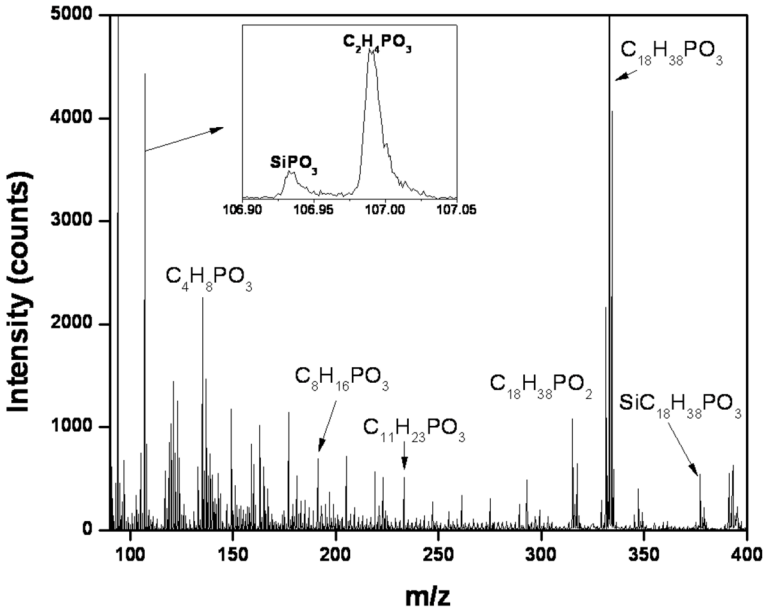

Figure 3.
Negative ToF-SIMS data from an ODPA modified silicon substrate.

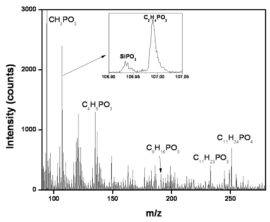

Figure 4.
Negative ToF-SIMS data from a PUL modified silicon substrate.

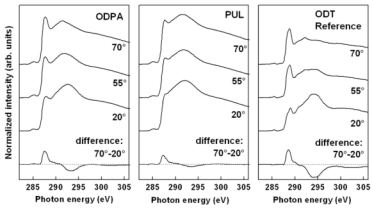

Figure 5.
NEXAFS spectra of the carbon *K*-edge for ODPA and PUL SAMs acquired at angles of 70°, 50° and 20° along with the difference between the 70° and the 20° spectra. The corresponding NEXAFS spectrum from an ODT SAM on gold is shown for comparison.

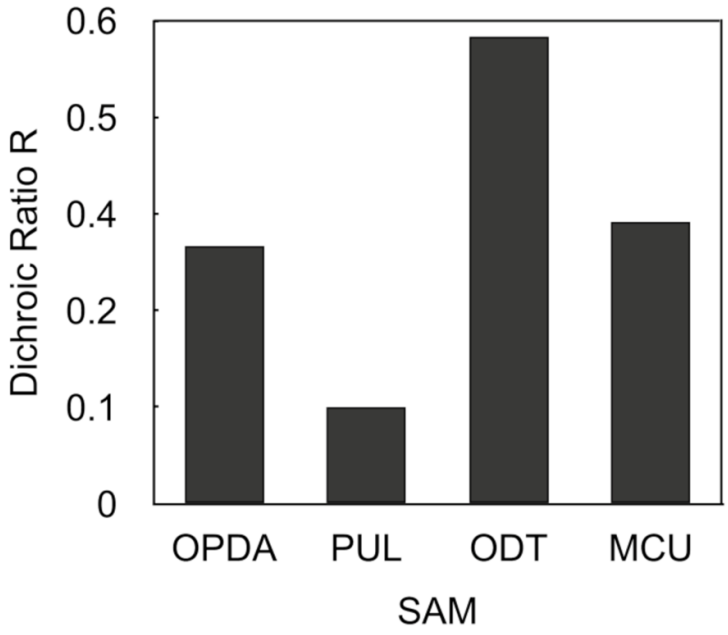

Figure 6.
Dichroic ratios R_I based on the R*/C-H σ* NEXAFS resonance intensities for the phosphonic acid SAMs on Si and the analogue thiol-based SAMs on Au.

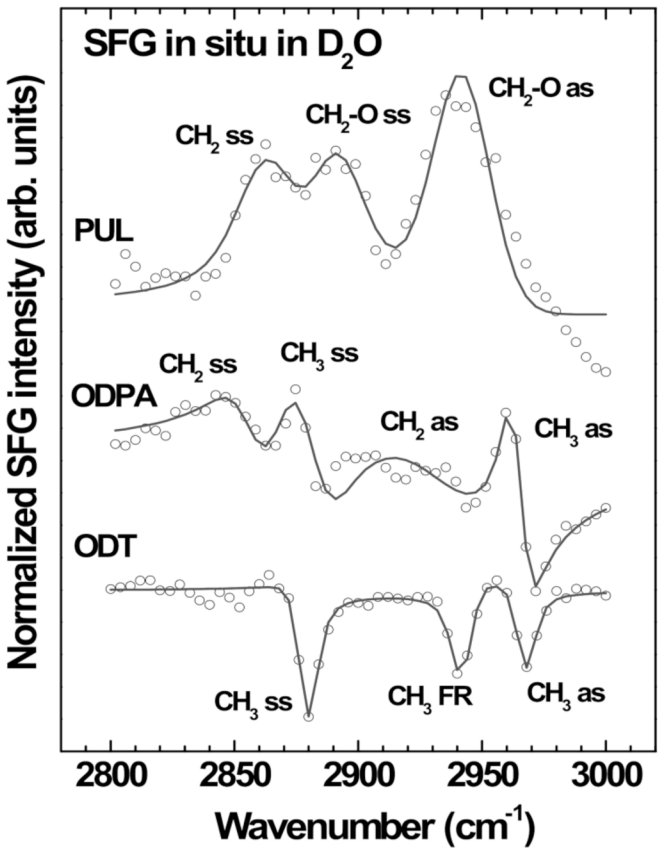

Figure 7.
SFG CH spectra of ODPA (upper trace) and PUL (middle trace) SAMs on Si(100) and a ODT SAM on gold (lower trace) taken *in situ* in D_2O. Solid lines are best fits to the SFG equation.

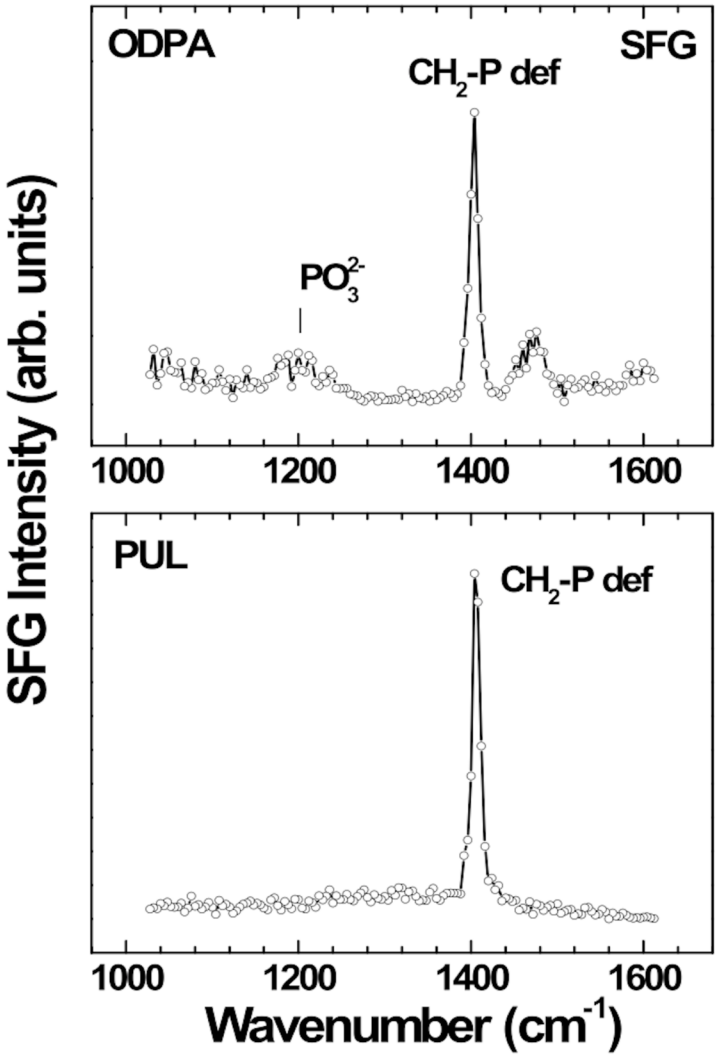

Figure 8.
Fingerprint region SFG spectra of ODPA (upper trace) and PUL (lower trace) SAMs on Si(100) taken *in situ* in D_2O.

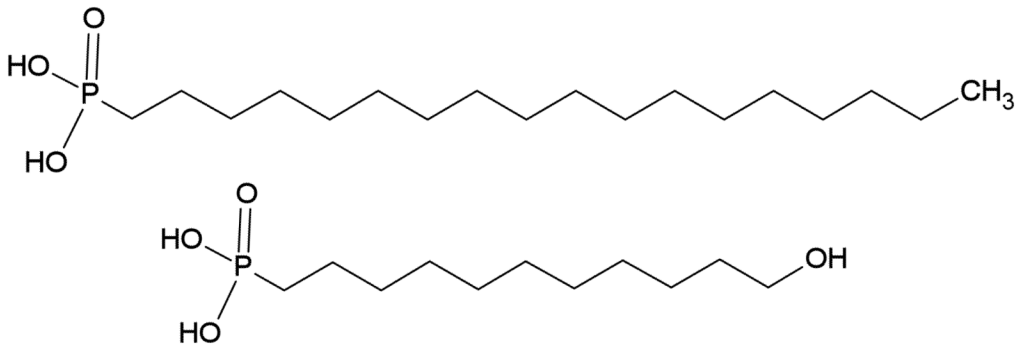

Scheme 1.
Structure of octadecylphosphonic acid (ODPA) and 11-hydroxyundecylphosphonic acid (PUL)

Table 1

The XPS determined relative compositions of SAM modified silicon and gold substrates, uncorrected for attenuation effects. Standard deviations are shown in parentheses.

Peak	Clean Si	Si-ODPA	Si-PUL	Au-ODT	Au-MCU
P2s	-	0.9 (0.2)	0.8 (0.3)	-	-
O1s	17.2 (1.2)	27.4 (1.1)	32.4 (2.1)	-	5.3 (1.6)
C 1s	9.3 (0.8)	18.6 (1.5)	12 (0.8)	62.8 (2.0)	45.5 (4.7)
Si2p	73.5 (2.5)	53.1 (1.7)	54.8 (2.0)	-	-
S2p	-	-	-	1.6 (0.3)	1.6 (0.7)
Au4f	-	-	-	35.6 (1.7)	47.6 (3.8)
C/P	-	21	15	-	-
C/S	-	-	-	39	28

Table 2

Characteristic ToF-SIMS positive and negative fragments for ODPA and PUL SAMs on silicon substrates.

ODPA peaks		PUL peaks	
Fragments	**Mass**	**Fragments**	**Mass**
Si^+	27.97	Si^+	27.97
$SiOH^+$	44.98	$SiOH^+$	44.98
Si_2O^+	71.95	Si_2O^+	71.95
$SiPO_2^+$	90.94	$SiPO_2^+$	90.94
$C_2H_6PO_3^+$	109.01	$C_2H_6PO_3^+$	109.01
$C_{18}H_{40}PO_3^+$	335.27	$C_{11}H_{22}PO_3^+$	233.12
$SiC_{18}H_{38}PO_3^+$	363.25		
		SiO^-	43.97
SiO^-	43.97	SiO_2^-	59.97
SiO_2^-	59.97	$CH_3PO_3^-$	93.98
$SiPO_3^-$	106.93	$SiPO_3^-$	106.93
$C_2H_4PO_3^-$	106.99	$C_4H_8PO_3^-$	135.02
$SiC_2H_4PO_3^-$	134.96	$C_8H_{16}PO_3^-$	191.08
$SiC_2H_8PO_3^-$	162.99	$C_{11}H_{23}PO_3^-$	234.14
$C_8H_{16}PO_3^-$	191.08	$C_{11}H_{24}PO_4^-$	251.14
$C_{11}H_{24}O_4P^-$	251.14		
$C_{18}H_{38}PO_2^-$	317.26		
$C_{18}H_{38}PO_3^-$	333.26		
$SiC_{18}H_{38}PO_4^-$	377.23		